Noninvasive Measurement of Vulnerability to Drought-Induced Embolism by X-Ray Microtomography[1]

Brendan Choat*, Eric Badel, Regis Burlett, Sylvain Delzon, Herve Cochard, and Steven Jansen

Hawkesbury Institute for the Environment, Western Sydney University, Richmond, New South Wales 2753, Australia (B.C.); Institut National de la Recherche Agronomique, Unité Mixte de Recherche 547 PIAF, F–63100 Clermont-Ferrand, France (E.B., H.C.); Université Blaise-Pascal, Unité Mixte de Recherche 547 PIAF, 63000 Clermont-Ferrand, France (E.B., H.C.); Institut National de la Recherche Agronomique, University of Bordeaux, Unité Mixte de Recherche BIOGECO, F–33450 Talence, France (R.B., S.D.); and Institute for Systematic Botany and Ecology, Ulm University, 89081 Ulm, Germany (S.J.)

ORCID IDs: 0000-0003-2282-7554 (E.B.); 0000-0001-8289-5757 (R.B.); 0000-0003-3442-1711 (S.D.).

Hydraulic failure induced by xylem embolism is one of the primary mechanisms of plant dieback during drought. However, many of the methods used to evaluate the vulnerability of different species to drought-induced embolism are indirect and invasive, increasing the possibility that measurement artifacts may occur. Here, we utilize x-ray computed microtomography (microCT) to directly visualize embolism formation in the xylem of living, intact plants with contrasting wood anatomy (*Quercus robur*, *Populus tremula* × *Populus alba*, and *Pinus pinaster*). These observations were compared with widely used centrifuge techniques that require destructive sampling. MicroCT imaging provided detailed spatial information regarding the dimensions and functional status of xylem conduits during dehydration. Vulnerability curves based on microCT observations of intact plants closely matched curves based on the centrifuge technique for species with short vessels (*P. tremula* × *P. alba*) or tracheids (*P. pinaster*). For ring porous *Q. robur*, the centrifuge technique significantly overestimated vulnerability to embolism, indicating that caution should be used when applying this technique to species with long vessels. These findings confirm that microCT can be used to assess the vulnerability to embolism on intact plants by direct visualization.

Theory describing the physiological mechanism that allows plants to extract water from the soil and transport it many tens of meters in height has often been the subject of intense debate (Tyree, 2003). Plants have evolved a water-transport system that relies on water sustaining a tensile force; as a result, xylem sap is at negative absolute pressures (Dixon and Joly, 1895; Melcher et al., 1998; Wei et al., 1999). However, this transport mechanism comes with its own set of problems. Most notably, water under tension is prone to cavitation, which results in the formation of gas bubbles (emboli) that block xylem conduits. Embolism reduces the capacity of the xylem tissue to deliver water to the canopy, where it is required to maintain adequate levels of cellular hydration (Tyree and Sperry, 1989). The probability of embolism occurring in the xylem increases during drought, with increasing tension in the xylem sap. During prolonged and severe droughts, xylem embolism can reach lethal levels, causing branch dieback and, ultimately, plant death (Davis et al., 2002; Brodribb and Cochard, 2009; Hoffmann et al., 2011; Choat, 2013; Urli et al., 2013). Water stress-induced embolism is now recognized as one of the principal causes of plant mortality in response to extreme drought events (Anderegg, 2015). In the face of increasingly severe droughts expected with rising global temperatures, hydraulic failure due to embolism has the potential to cause widespread dieback of trees across all major forest biomes (Choat et al., 2012).

The majority of techniques used to estimate cavitation resistance are indirect and/or invasive, increasing the possibility of artifacts occurring during measurement (Cochard et al., 2013). Artifacts relating to invasive techniques are particularly relevant in this case, since xylem sap under tension is in a metastable state and may easily vaporize as a result of disturbance. Noninvasive imaging techniques offer the potential to make direct observations of xylem function in intact plants at high resolution and in real time. Noninvasive techniques include magnetic resonance imaging (MRI; Holbrook et al., 2001; Kaufmann et al., 2009; Choat et al., 2010) and, more recently, x-ray computed microtomography

[1] This work was supported by the European Research Council under Advanced Grant Project TREEPEACE (grant no. FP7–339728), by the French National Agency for Research (Investments for the Future Program grant no. ANR–10–EQPX–16, XYLOFOREST, and French Pitbulles Program grant no. ANR–10–BLAN–1710 to H.C. and E.B.), by the Australian Research Council (Future Fellowship grant no. FT130101115 to B.C.), and by the International Synchrotron Access Program managed by the Australian Synchrotron.

* Address correspondence to b.choat@westernsydney.edu.au.

The author responsible for distribution of materials integral to the findings presented in this article in accordance with the policy described in the Instructions for Authors (www.plantphysiol.org) is: Brendan Choat (b.choat@westernsydney.edu.au).

All authors contributed to experimental design, research planning, and experiments; B.C. wrote the article with contributions from all authors.

www.plantphysiol.org/cgi/doi/10.1104/pp.15.00732

(microCT; Brodersen et al., 2010; Charra-Vaskou et al., 2012; McElrone et al., 2012). MicroCT provides superior spatial resolution to MRI, with resolutions below 2 μm attainable for a plant stem of 4 to 5 mm in diameter. This allows for detailed analysis of embolism formation and repair in the xylem, including spatial patterns of embolism spread between conduits (Brodersen et al., 2013; Dalla-Salda et al., 2014).

However, noninvasive imaging techniques have seldom been used to validate indirect or invasive techniques used to estimate cavitation resistance. At this stage, only a handful of studies have utilized imaging technology to measure cavitation resistance in trees (Torres-Ruiz et al., 2014; Cochard et al., 2015), and these studies employed a destructive mode of the technique in which small branches were cut off the plant before scanning took place. Thus far, noninvasive imaging on intact plants has only been used to measure cavitation resistance in two species, grapevine (*Vitis vinifera*; Choat et al., 2010; Brodersen et al., 2013) and *Sequoia sempervirens* (Choat et al., 2015). Further measurement of cavitation resistance using noninvasive imaging on intact plants across a range of species, therefore, is a high priority.

These comparisons are particularly important because of the current debate surrounding the invasive techniques (Cochard et al., 2013). Specifically, evidence from a variety of experiments suggests that centrifuge and air injection techniques underestimate cavitation resistance in species with long xylem vessels (Choat et al., 2010; Cochard et al., 2010; Ennajeh et al., 2011; Martin-StPaul et al., 2014; Torres-Ruiz et al., 2014; Wang et al., 2014). This artifact occurs when samples placed into centrifuge rotors or air injection collars have a large proportion of vessels that are cut open at both ends of the segment. A number of studies have disputed this open-vessel hypothesis and suggested that some versions of the centrifuge and air injection techniques provide reliable estimates of cavitation resistance (Jacobsen and Pratt, 2012; Sperry et al., 2012; Tobin et al., 2013). Because there will always be uncertainties associated with indirect measurements, noninvasive imaging using intact plants provides the best option for resolving these methodological issues.

In this study, synchrotron-based microCT was utilized to investigate the formation of drought-induced embolism in the xylem of intact, potted plants. Three species were selected to provide a range of contrasting xylem structures: *Quercus robur* (ring porous), *Populus tremula* × *Populus alba* (diffuse porous), and *Pinus pinaster* (tracheid bearing). Visualizations of xylem embolism in the stems of these species during a sequence of natural dehydration were used to construct embolism vulnerability curves. We hypothesized that (1) vulnerability curves based on microCT observations would match vulnerability curves based on the centrifuge technique for species with short vessels (*P. tremula* × *P. alba*) or tracheid-based xylem (*P. pinaster*) and (2) the centrifuge technique would overestimate vulnerability to embolism in the long-vesseled species (*Q. robur*) due to the open-vessel artifact.

RESULTS

Vulnerability curves generated with the centrifuge method were in close agreement with curves generated from microCT observations for *P. tremula* × *P. alba* and *P. pinaster* (Fig. 1; Table I). For these two species, P_{50} was not significantly different ($P > 0.05$) between curves generated by the microCT and Cavitron techniques. The estimates of P_{50} obtained for *Q. robur* by the Cavitron method (−1.38 MPa) and static centrifuge (−0.47 MPa) were significantly higher ($P < 0.05$) than the P_{50} obtained

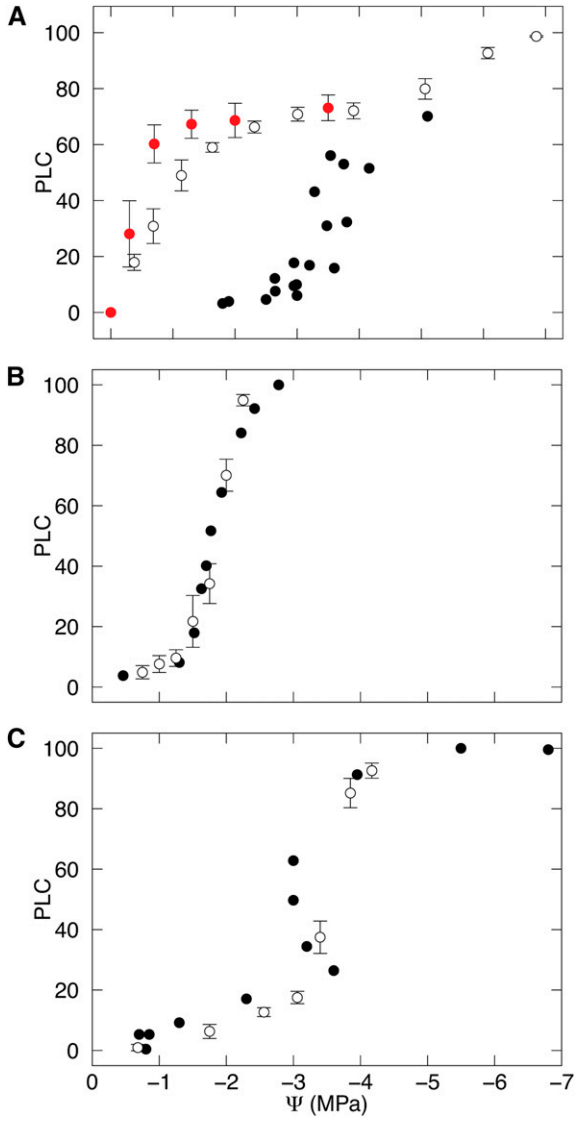

Figure 1. Vulnerability to drought-induced embolism in three woody plant species with contrasting xylem structure. Vulnerability to embolism is shown for *Q. robur* (A), *P. tremula* × *P. alba* (B), and *P. pinaster* (C). Percentage loss of conductivity (PLC) is plotted against stem water potential (Ψ) for each species. PLC was determined by microCT observations (black symbols), Cavitron (white symbols), and static centrifuge (red symbols). Error bars for centrifuge data show SE for each pressure (n = 3–5).

Table I. *Xylem pressure at 50% loss of hydraulic conductance (P_{50}) for three woody species as determined by two centrifuge techniques and microCT*

Within each row, different letters indicate significant differences ($P < 0.05$) across techniques. Values are means ± SE (n = 3–5 for Cavitron and static centrifuge measurements).

Species	Cavitron	Static Centrifuge	MicroCT
		−*MPa*	
Q. robur	1.38 ± 0.10 a	0.47 ± 0.09 b	4.16 ± 0.16 c
P. tremula × *P. alba*	1.83 ± 0.05 a		1.81 ± 0.02 a
P. pinaster	3.50 ± 0.06 a		3.27 ± 0.23 a

from microCT observation (−4.1 MPa; Table I). This difference was due to variation in curve shape; the centrifuge curves for *Q. robur* exhibited a characteristic exponential shape curve in which PLC increased rapidly at high water potentials. Although both centrifuge curves for *Q. robur* were exponential in form, the P_{50} derived from the static centrifuge method was significantly ($P < 0.05$) higher than that derived from the Cavitron (Table I). All other curves were sigmoidal, with PLC remaining close to zero until a critical threshold was reached. Vessel length analysis revealed that 19% ± 5% (SE) of vessels were cut open at both ends of a 0.275-m-long segment of *Q. robur*. For *P. tremula* × *P. alba*, no vessels were cut open at both ends of the 0.275-m-long segment.

Two- and three-dimensional analyses of microCT scan volumes provided detailed information on the propagation of xylem embolism during dehydration. In each of the three xylem types, ring porous, diffuse porous, and conifer, a very small percentage of secondary xylem conduits were embolized at high water status in the initial scans (Fig. 2). These embolized conduits often appeared to be isolated from other embolized conduits within the scan volume, although this could only be confirmed for *P. pinaster* (Fig. 3), because vessels in *Q. robur* and *P. tremula* × *P. alba* extended out of the scan volume. In *P. pinaster* xylem, embolism appeared first in the primary xylem adjacent to the pith and then in the inner ring of latewood tracheids. Embolized tracheids were also frequently located adjacent to resin ducts (Fig. 2). In both angiosperm and gymnosperm species, the majority of primary xylem conduits were usually embolized at high water status and prior to the first scan (Supplemental Fig. S1). With dehydration and increasing xylem tension, embolism spread from the initially embolized conduits to create patches of embolized xylem throughout the cross section (Fig. 4). As dehydration continued, these patches gradually converged until almost all conduits were embolized (Fig. 4).

DISCUSSION

Synchrotron-based microCT produced excellent visualization of xylem tissue in three woody plant species of differing xylem structure. Making observations on living, intact plants avoided previously identified artifacts associated with cutting (Wheeler et al., 2013; Torres-Ruiz et al., 2015) and the presence of open vessels (Cochard et al., 2010). The high quality of signal and contrast allowed for the measurement of xylem conduit dimensions to a resolution of 1.62 μm for both air- and water-filled conduits. This offers a dramatic improvement over MRI, which has been used previously for noninvasive assays of xylem function, with spatial resolutions down to 20 to 40 μm (Holbrook et al., 2001; Kaufmann et al., 2009; Choat et al., 2010; Wang et al., 2013). In the context of measuring vulnerability to embolism, one key benefit of achieving resolutions close to 1 μm is the ability to calculate theoretical hydraulic conductance from conduit dimensions. The impact of xylem embolism on hydraulic capacity, therefore, can be estimated with a much greater degree of confidence. MicroCT thus provides a direct and unambiguous assay of xylem functional status and serves as an excellent reference technique to assess the reliability and accuracy of destructive techniques used to estimate vulnerability to embolism (Cochard et al., 2015).

Comparison of Methods to Assess Vulnerability to Embolism

Vulnerability curves generated by the microCT observations closely matched the curves based on the Cavitron technique for *P. tremula* × *P. alba* and *P. pinaster*. This demonstrates conclusively that the Cavitron technique provides an accurate and precise measure of vulnerability to embolism in these species. In contrast, centrifuge techniques significantly overestimated the vulnerability to embolism in *Q. robur*, particularly in the range of xylem water potentials from −0.25 to −2.5 MPa.

The converse argument, that microCT observations underestimated vulnerability in *Q. robur*, is unlikely but bears further discussion. One possibility is that the x-ray beam may cause cavitation in dehydrating samples, either by heating or x-ray absorption. However, we did not observe any cavitation resulting from repeated scans at the same scan point (Supplemental Fig. S2). Furthermore, this artifact would be expected to cause differences in vulnerability that were in the opposite direction from those observed (i.e. microCT curves would exhibit greater vulnerability than hydraulic methods). A second possibility is that noninvasive imaging underestimates embolism because many of the cells that appear water filled are still living and, therefore, nonfunctional (Jacobsen and Pratt, 2012). In this case, all microCT observations were made late in the growing season, so undifferentiated and immature

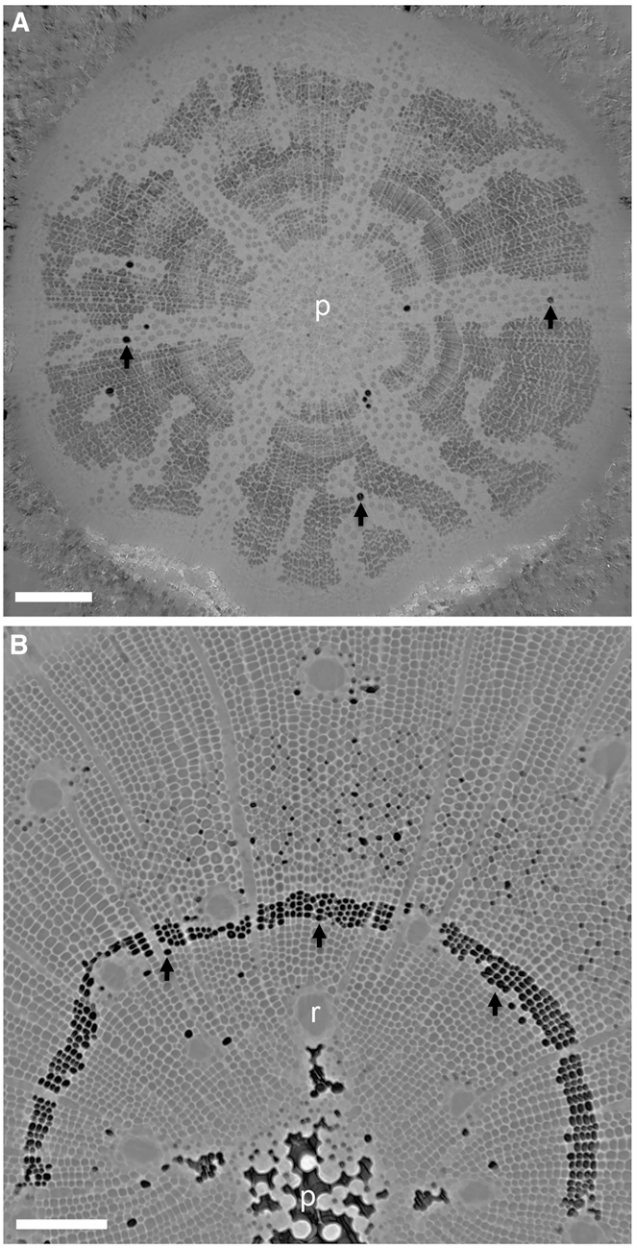

Figure 2. Transverse slices from microCT scans show examples of xylem conduit functional status at the initial scan point for saplings of *Q. robur* (A) and *P. pinaster* (B). Embolized conduits appear as black space (black arrows), while water-filled conduits appear gray. In *Q. robur*, vessels occur in dendritic bands surrounded by water-filled tracheids. Fibers surrounding the dendritic bands were air filled from the initial scan point. The pith (p) contained large air-filled spaces in *P. pinaster* but not in *Q. robur*. A band of embolized latewood tracheids from the previous year's growth was often present in the initial scans of *P. pinaster* (black arrows). Resin canals (r) were also visible in the stems of *P. pinaster*. The water potentials of these samples at the time of scanning were −1.9 MPa for *Q. robur* and −0.8 MPa for *P. pinaster*. Bars = 500 μm for A and 200 μm for B.

conduits would be expected to make up only a very small proportion of the total stem in the juvenile wood of saplings.

Excising leaves in air for the measurement of bagged leaf water potential has the potential to create embolism in the stem xylem, although the extent was very limited in older sections of the stem. Removal of up to seven leaves did not result in new cavitation in the 2-year section of the stem close to the base of the plant (Supplemental Fig. S2). This indicates that water potential measurements in our initial experiments would have a very limited effect on PLC calculated from microCT imaging, given that all scans were made more than 0.2 m below the point where leaves were collected for water potential measurements. However, the removal of leaves consistently caused embolism in the xylem of current-year stems when cuts were made within 0.05 m of the scan point. Overall, these results indicate that care must be taken when scans are made close to the point of leaf removal and that the number of leaves collected for water potential measurements should be minimized. They also suggest that alternative techniques for the measurement of water potential that do not require damage to the xylem (e.g. stem psychrometry and leaf disc psychrometry) should be considered for these experiments.

The results shown here for *Q. robur* are also consistent with earlier findings that centrifuge techniques overestimate the vulnerability to embolism in species with long vessels and provide further support for the open-vessel artifact hypothesis (Choat et al., 2010; Cochard et al., 2010; McElrone et al., 2012; Martin-StPaul et al., 2014; Torres-Ruiz et al., 2014). Consistent with this, measurements of *Q. robur* saplings indicated that over 19% of vessels were cut open at both ends in stem segments used for centrifuge measurements. The most likely cause of this artifact is that microbubbles, which move into the sample either prior to, or during, the spinning phase lead to embolism formation when they reach the center of the sample where centrifugal forces are highest (Wang et al., 2014). This open-vessel artifact has been the subject of intense debate, with some researchers suggesting that the artifact only affects the Cavitron version of the centrifuge technique and not the static centrifuge method (Christman et al., 2012; Jacobsen and Pratt, 2012; Sperry et al., 2012; Tobin et al., 2013; Hacke et al., 2015). Data from this study demonstrate that static and spin centrifuge techniques produced similarly biased results for *Q. robur*. This finding agrees with previous work indicating that all centrifuge techniques overestimate vulnerability to embolism in long-vesseled species when compared with reference curves generated by dehydration or noninvasive imaging (Torres-Ruiz et al., 2014). The higher P_{50} observed with the static centrifuge as compared with the Cavitron is most probably due to variation in vessel length between samples (Wang et al., 2014).

Based on these results, we reiterate that caution should be used when applying centrifuge-based techniques to samples in which a large proportion of vessels are cut open at both ends of the segment. In the case of conifers, there is no possibility that tracheids will exceed the length of the rotor used in centrifuge measurements.

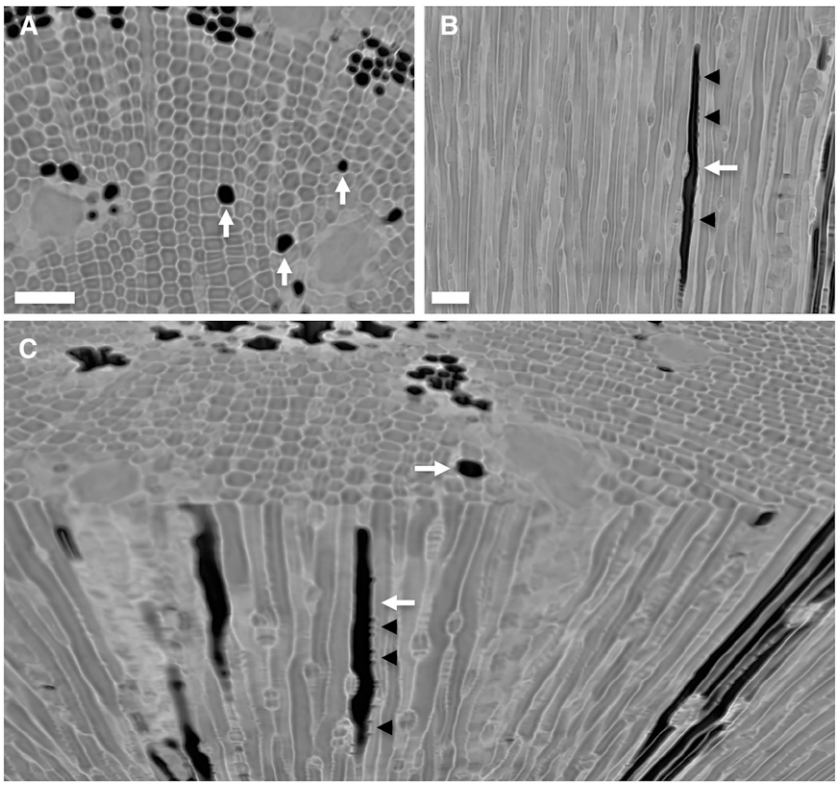

Figure 3. Imaging from microCT scans demonstrating the presence of isolated, embolized tracheids (white arrows) in the stem xylem of *P. pinaster* for a transverse slice (A), a longitudinal slice (B), and a three-dimensional rendering showing transverse and longitudinal views together (C). Gas in bordered pit chambers connecting an embolized and a functional tracheid can be observed in longitudinal slices (black arrowheads). Isolated tracheids were not connected to other resolvable gas-filled spaces in the xylem of intact plants. Bars = 50 μm.

Although the microCT vulnerability curve was almost identical to the centrifuge curve for *P. tremula* × *P. alba*, caution is still advised for diffuse porous species, since vessel lengths are highly variable (Zimmermann and Jeje, 1981; Sperry et al., 2006) and may exceed rotor diameter in some cases.

Patterns of Embolism Spread with Dehydration

Three-dimensional analysis of scan volumes illustrated the fine spatial patterns of embolism spread within each xylem type. These spatial analyses suggest that air seeding through pit membranes was the dominant mechanism of cavitation in all three xylem types. However, a small number of isolated, embolized conduits were observed in both vessel- and tracheid-bearing species, suggesting that other mechanisms of cavitation may also operate in the xylem (Fig. 3; Supplemental Fig. S1).

The majority of primary xylem conduits were embolized at high water status in each of the three species (Supplemental Fig. S1). This is similar to the pattern observed in intact grapevine using MRI (Choat et al., 2010) and microCT (Brodersen et al., 2013) and extends this earlier finding across a range of xylem types. Single-vessel measurements indicate that protoxylem conduits are more vulnerable to air seeding because they possess only partial secondary wall thickening and may suffer damage during extension growth, which can cause stretching and rupture of the primary cell walls (Choat et al., 2005). The secondary xylem of all species also contained a number of embolized conduits at the initial scan point. These embolized conduits often appeared to be isolated from other air-filled spaces within the scan volume. However, in the vessel-bearing species (*Q. robur* and *P. tremula* × *P. alba*), vessels were always longer than the length of the scan volume (approximately 5 mm). Therefore, it was not possible to verify whether apparently isolated embolized conduits were actually connected to other embolized conduits outside the scan volume. There were also numerous embolized tracheids visible in the initial scans of *P. pinaster* stems that were isolated from other air-filled tracheids (Supplemental Fig. S1). In this case, we were able to verify that these embolized tracheids were completely isolated from other air spaces because tracheid lengths were less than the scan volume (Fig. 3). This suggests that these tracheids may have become embolized by a mechanism other than air seeding (e.g. defects in wall structure during initial formation, nucleation from hydrophobic surface, or vapor embryos; Pickard, 1981; Tyree et al., 1994; Schenk et al., 2015). This is consistent with the results of microCT observations on intact saplings of *S. sempervirens*, which also indicated the presence of isolated, embolized tracheids (Choat et al., 2015).

With dehydration and increasing xylem tension, embolism spread from the initially embolized vessels and tracheids. This pattern is consistent with air seeding through pit membranes as the primary mechanism of cavitation in the xylem (Zimmermann, 1983; Sperry and Tyree, 1988; Cochard et al., 1992; Choat et al., 2008).

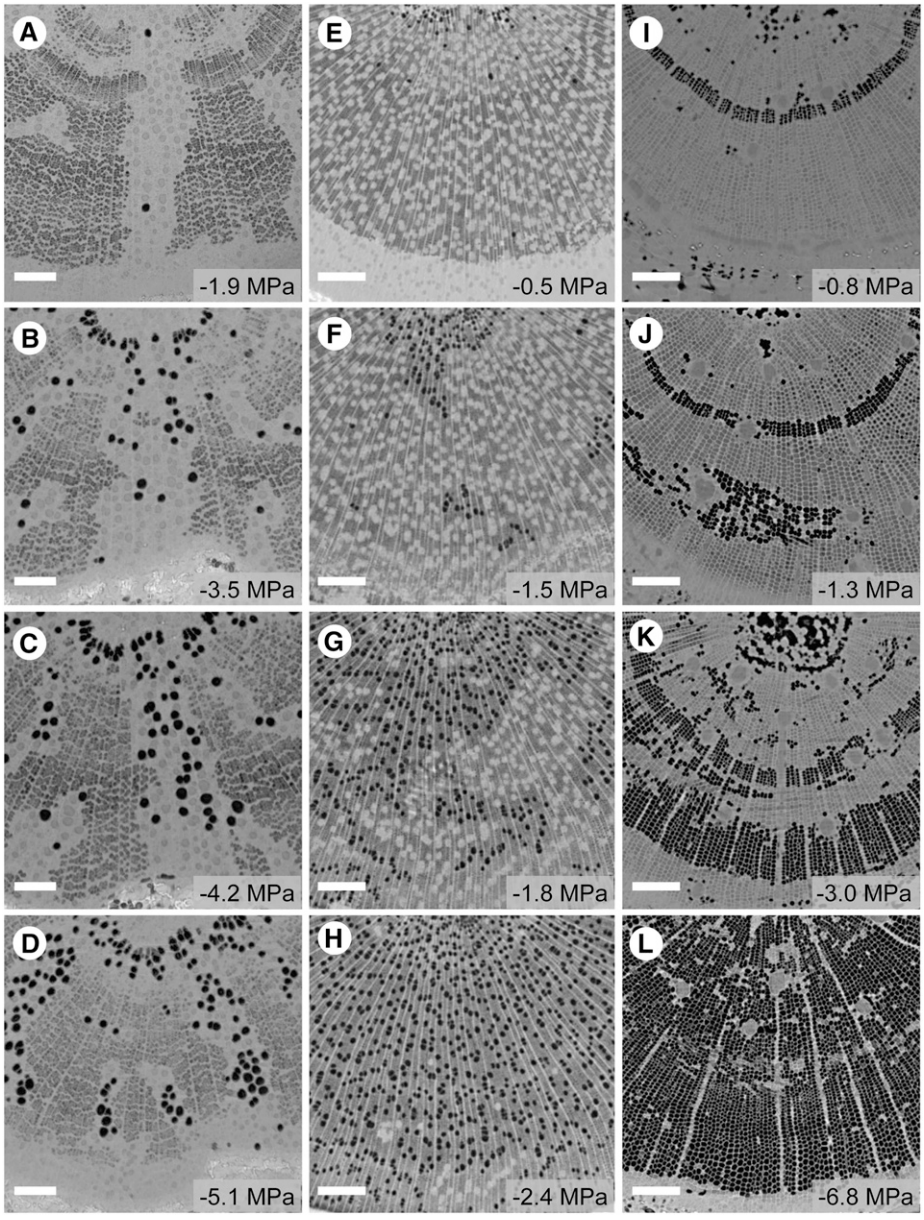

Figure 4. Visualization by microCT showing the progressive spread of embolism in the xylem of three woody plant species during dehydration: *Q. robur* (A–D), *P. tremula* × *P. alba* (E–H), and *P. pinaster* (I–L). Embolized conduits appear as black space in the cross section, while water-filled conduits appear as light gray. Each column shows transverse slices through the main stem axis with increasing water stress down the column. The bagged leaf water potential of each sample at the time of scanning is given at bottom right. Bars = 200 μm.

Although embolism was more frequent in the inner portions of the stem during the early stages of dehydration, this pattern was not as distinct as the radial spread of embolism observed in grapevine stems (Brodersen et al., 2013). In *Q. robur*, dendritic bands of tracheids surrounding vessels and ray cells remained hydrated for the duration of the experiment. In contrast, fiber cells were always observed to be air filled. In the xylem of *P. tremula* × *P. alba*, fibers surrounding the vessels were also embolized, with the exception of a band close to the cambium (Fig. 4). This is similar to the distribution of water observed by cryo-scanning electron microscopy in the xylem of diffuse porous species growing under well-watered conditions (Utsumi et al., 1998). As *P. tremula* × *P. alba* stems dehydrated, the water-filled fibers close to the cambium gradually embolized.

In *P. pinaster* xylem, embolism appeared first in the primary xylem adjacent to the pith and then in the inner ring of latewood tracheids (Fig. 2). This is consistent with observations of xylem from mature Douglas fir (*Pseudotsuga menziesii*) trees, which also demonstrates the much higher vulnerability of latewood tracheids compared with earlywood (Dalla-Salda et al., 2014). Latewood tracheids may be more vulnerable to embolism because of their pit structure. Anatomical work has shown that the margo in latewood tracheids of many conifer species are inflexible and do not readily allow the torus to seal the pit aperture in the event of air entry (Domec et al., 2006). This is also apparent from the work of wood technologists, who have shown that latewood remains unaspirated in dried wood samples (Petty, 1970). Embolism spread primarily in the lateral direction,

presumably because intertracheid pits are located almost exclusively on the radial walls of tracheids. It is likely that much of this embolism spread from the initially isolated embolized tracheid and small patches of tracheids adjacent to resin ducts. Embolism then spread in a noncontiguous fashion between rings, with some earlywood tracheids in the outer rings becoming embolized. This pattern of embolism spread suggests differential resistance to cavitation along files of tracheids in the growth ring, most probably related to variation in pit level traits (Pittermann et al., 2010; Dalla-Salda et al., 2014). Embolism then spread outward to the cambium and back toward the pith until the majority of tracheids were embolized.

CONCLUSION

The results of microCT observations confirm that this technique is an excellent noninvasive method for the measurement of vulnerability to embolism, with the principal advantage that measurements can be made on intact plants. The high resolution of images allowed for the calculation of theoretical hydraulic conductivity based on xylem conduit dimensions. Therefore, we were able to estimate the impact of embolized vessels and tracheid on the hydraulic capacity of each sample. The fine spatial patterns of embolism spread within the xylem could also be followed, providing insight into the way cavitation is nucleated within the xylem. The results indicated that centrifuge techniques overestimated vulnerability to embolism in ring-porous *Q. robur*, consistent with previous reports suggesting that the centrifuge suffers from an open-vessel artifact when applied to long-vesseled species (Choat et al., 2010; Cochard et al., 2010; Torres-Ruiz et al., 2014). However, the centrifuge produced curves that were in excellent agreement with microCT observations for diffuse porous *P. tremula* × *P. alba* and the conifer *P. pinaster*. These results provide further evidence that the centrifuge technique is a rapid and reliable method of assessing vulnerability to embolism in species with short vessels or tracheids but is prone to errors when a high proportion of vessels are cut open in the measurement sample. Caution is advised when applying this technique to species with vessel lengths that exceed the diameter of the rotor used in centrifuge methods.

MATERIALS AND METHODS

Plant Material

Ten 2-year-old *Quercus robur* and five 1-year-old *Populus tremula* × *Populus alba* (clone INRA 717-1B4) saplings were grown at the laboratories of the Institut National de la Recherche Agronomique in Bordeaux (44°44′N, 00°46′W) and Clermont-Ferrand (45.76°N, 3.14°E), respectively. *Q. robur* seeds were collected in a natural population in southern France, while *P. tremula* × *P. alba* plants were multiplied clonally by in vitro micropropagation. After potting, the plants were gradually acclimatized in a greenhouse under well-watered conditions (irrigated twice daily at ambient light and temperature). At the time of measurement, sapling stems ranged between 0.4 and 0.8 m high with an average diameter of 4.5 mm at the base. Plants were moved to the Swiss Light Source (SLS; Paul Scherrer Institute) and scanned in September 2012.

In July 2013, 50 *Pinus pinaster* saplings were ordered from PlanFor nursery. All plants were 2 years old at the time of purchase. Plants were repotted into 0.7-L pots and grown for 1 month under well-watered conditions (irrigated twice daily at ambient light and temperature) at the Ulm University Botanical Gardens (48.4222°N, 9.9539°E). Plants were moved to the SLS and scanned in September 2013. Two weeks prior to the microCT imaging, drought stress was induced in 20 plants by cessation of irrigation. In order to facilitate dehydration vulnerability curves, plants were dried for varying periods to produce a range of stem water potentials. At the time of measurement, plants were 0.2 to 0.3 m in height and 3 to 5 mm diameter at the stem base. Measurements using the static centrifuge technique were applied to another set of 2-year-old *Q. robur* saplings in March 2015. These saplings were grown in the greenhouse under identical conditions to the first cohort of *Q. robur* seedlings. A third cohort of *Q. robur* saplings, which had been raised outside of the greenhouse, was used for the evaluation of leaf removal in microCT experiments.

MicroCT

Synchrotron-based microCT was used to visualize embolized and water-filled conduits in the main stem axes for each of the three species. Potted plants were transported to the SLS tomography beamline (TOMCAT-X02DA). Tomographic scans were recorded during two allocations of beamtime. *Q. robur* and *P. tremula* × *P. alba* plants were visualized in September 2012, while observations of *P. pinaster* were recorded in September 2013.

The measurement protocol used to scan living plants is described in detail by McElrone et al. (2013). Potted plants were placed in a custom-built aluminum holder that immobilized the stem and mounted on the TOMCAT sample stage. For each plant, a 5-mm section of the main stem axis was scanned approximately 0.03 m above the soil surface. Stems were positioned 30 mm from the two-dimensional detector and secured to bamboo or birch wood skewers (3 mm diameter) in order to minimize sample movement during rotation of the stage. Plants were scanned at 20 keV in the synchrotron x-ray beam while being rotated through 0° to 180° using continuous rotation mode. X-ray projections were collected at 0.12° steps with 150-ms exposure time during rotation, with projection images magnified through a series of lenses and relayed onto an sCMOS camera (pco.edge 5.5; PCO). The scan time was less than 4 min for each sample. Samples were removed between scans and placed under light-emitting diode lighting to facilitate more rapid drying of plants.

Scans yielded 1,500 two-dimensional projections per sample. Raw two-dimensional tomographic projections were reconstructed into a single three-dimensional volume that was then split into approximately 2,000 TIF image slices using software developed at the TOMCAT beamline. This yielded images with a 1.625-μm voxel resolution. These images were analyzed in ImageJ (Rasband, 2014) and Avizo 8.1.1 software (VSG) to determine the location and dimensions of embolized vessels or the cross-sectional area of embolized tracheids within each sample.

For *Q. robur* and *P. tremula* × *P. alba*, scans were made on five plants per species, with plants scanned every 3 h during dehydration. Plants were dried in pots under laboratory conditions at the SLS facility. A red-blue light-emitting diode light source was secured 1 m above the potted plants. A fan was also used to increase the rate of dehydration in *Q. robur* plants. *P. pinaster* plants were dehydrated at the Ulm University Botanical Gardens prior to arrival at the SLS. In August 2013, plants were moved to a rainout shelter and divided into four groups. Water was withheld for 1, 2, or 3 weeks prior to scanning, respectively, for three of the groups. The fourth group was maintained in well-watered conditions. Each plant was scanned once at the SLS.

Covered leaf water potential was measured on leaves or leafy twigs just prior to scans using a Scholander Pressure Chamber (Plant Moisture Stress model 600). Leaves were covered with plastic bags and aluminum foil for at least 30 min prior to each measurement of water potential. Due to concerns regarding the impact of leaf removal for water potential measurements on cavitation in the stem xylem, another set of observations was undertaken in April 2015 at the SOLEIL microCT beamline at PSICHÉ. These measurements were conducted on 2-year-old *Q. robur* plants grown at the laboratories of the Institut National de la Recherche Agronomique in Bordeaux (44°44′N, 00°46′W). Plants were first scanned in the 2-year-old section of the stem before any leaves were removed. After 15 min, plants were scanned again at the same point to test whether the x-ray beam itself was causing cavitation. A leaf was then removed from the apex of the plant, between 0.2 and 0.25 m above the scan point, and the plant was scanned for a third time after a further 15 min. The plant holder was then moved down, and the procedure was repeated at a scan point on the current-year shoot within 0.03 to 0.05 m of where leaves would be removed for water potential measurements. This protocol was applied to two replicate plants. These measurements indicated that (1) the x-ray beam did not induce cavitation in the stem

during scans and (2) the removal of leaves for water potential measurements had the potential to induce air entry and embolism in xylem vessels, although only in the current-year growth zone within 6 cm of where the leaf was removed (Supplemental Fig. S2).

Vulnerability Curves Based on microCT Observations

Vulnerability curves were generated from microCT by estimating the theoretical hydraulic conductance of each sample based on the conduit dimensions of embolized and functional conduits. Measurements were made on transverse slices taken from the center of the scan volume. For angiosperm species, vessel diameters were measured manually. To increase the accuracy of vessel diameter measurements, a final scan was carried out on each stem after it had been cut in air. This ensured that all vessels were air filled at the time of scanning, increasing the contrast with surrounding tissue. For *P. pinaster* samples, a binary image was created for each transverse slice, and the dimensions of tracheids were automatically measured using the analyze particles function. A separate run was required to separate embolized from functional tracheids. The watershed function was used to assist in separating tracheids that were connected after the initial thresholding (Choat et al., 2007).

The maximum theoretical hydraulic conductance (k_{max}) of each stem was then calculated as:

$$k_{max} = \sum \pi D^4 / 128\eta \quad (1)$$

The current hydraulic conductance (k_h) for each sample was then calculated by subtracting the summed hydraulic conductance of embolized vessels from the k_{max} of that sample. This calculation of hydraulic conductance does not include the hydraulic resistance due to pits. Assuming that pit resistance scales with lumen resistance (Choat et al., 2008), the impairment of flow calculated with Equation 1 should be comparable with flow rates measured directly on the plant. Therefore, the theoretical percentage loss of hydraulic conductance (PLC_{th}) of the sample was given by:

$$PLC_{th} = 100 \times (1 - k_h/k_{max}) \quad (2)$$

In all cases, measurements included all secondary xylem visible in the cross section of a given sample. Primary xylem was excluded from calculations on the basis that it had become embolized previously in the majority of cases. Curve fitting and analysis of curve parameters are described below.

Vulnerability Curves Based on Hydraulic Measurements

Vulnerability to xylem cavitation was assessed using two versions of the centrifuge technique: the static centrifuge method described by Alder et al. (1997) and the in situ flow technique (Cavitron) developed by Cochard (2002) and Cochard et al. (2005). Both techniques employ centrifugal force to generate tension in the xylem of spinning stem samples. In the Cavitron technique, the loss of hydraulic conductance is measured while the sample is spinning (under tension) in the centrifuge. In the static centrifuge technique, the sample is removed between spins to measure hydraulic conductance on the bench top. The in situ flow and static versions of the centrifuge technique have been shown to produce similar results (Li et al., 2008; Torres-Ruiz et al., 2014). All hydraulic measurements were made with 10 mM KCl solution filtered to 0.2 μm.

Cavitron measurements were carried out on all three species, while static centrifuge measurements were conducted only on *Q. robur*. Cavitron measurements were conducted on the same population of 2-year-old *Q. robur* plants as used for microCT observations directly after the 2012 SLS beamtime allocation. Four-year-old *P. pinaster* plants were measured with the Cavitron in May 2010. Three to five replicates were measured per species at a high-throughput phenotyping platform for hydraulic traits (Cavit_Place; University of Bordeaux). Measurements were made using a custom-built honeycomb rotor (SamPrecis 2000) mounted on a Sorvall RC5 superspeed centrifuge (Thermo Fisher Scientific). Cavitron vulnerability curves shown for *P. tremula* × *P. alba* clone INRA 717-1B4 are based on data from Awad et al. (2010). Samples of *Q. robur* and *P. pinaster* were cut under water to a length of 0.27 m to fit into the static Cavitron rotor. For *Q. robur*, samples were flushed at approximately 0.15 MPa to remove any embolism until a stable maximum hydraulic conductance value was reached prior to measurements.

Xylem pressure was first set to a reference pressure (−0.4 to −0.6 MPa), and the maximal conductance of the sample was determined once a stable value had been reached. The xylem pressure was then set to a more negative value for 3 min, and the hydraulic conductance of the sample was again determined. The PLC at each pressure step was calculated as per Equation 2. The procedure was repeated for more negative pressures (with 0.5- to 1-MPa increments) until PLC reached at least 90%.

Measurements using the static centrifuge technique were applied to another set of 2-year-old *Q. robur* saplings in March 2015. Samples were spun to five xylem tensions ranging between −0.3 and −3.5 MPa. Foam pads saturated with perfusing solution were added to reservoirs in the centrifuge rotor in order to ensure that the cut ends of samples remained immersed in water during spinning (Hacke et al., 2015). Measurements of hydraulic conductance between spins were made using a Sartorious Practum analytical balance (0.01 mg resolution) connected to a computer with a custom program recording flow and computing conductance (Graviflow; University of Bordeaux). Hydraulic conductance was calculated from the slope of three pressure heads (0.13, 0.17, and 0.2 m) following the protocol described by Torres-Ruiz et al. (2012). Pressure heads were kept low (less than 0.0021 MPa) to avoid the removal of embolism from open vessels during flow measurements. All measurements were made on the whole sample (0.27 m length) after at least 2 min of stable flow.

To facilitate the comparison of Cavitron and static centrifuge vulnerability curves for *Q. robur*, the k_{max} of Cavitron measurements was calculated by extrapolating from the first three measurements in the pressure series to the *y* intercept. This provided an estimate of k_{max} at a pressure of 0 MPa. This was necessary because the first Cavitron measurement of k_h was taken at −0.3 MPa, a point at which substantial PLC had already occurred in the static centrifuge measurements. The offset calculated for Cavitron k_{max} allowed for both curves to be scaled to k_{max} at pressure = 0 MPa. A plot of sapwood-specific hydraulic conductivity versus xylem pressure is provided in Supplemental Figure S3.

Curve Fitting

All vulnerability curves were fitted using a Weibull function as reparameterized by Ogle et al. (2009):

$$k = k_{sat}\left(1 - \frac{X}{100}\right)^p$$
$$p = \left[\left(\frac{P}{P_x}\right)^{\frac{P_x S_X}{V}}\right] \quad (3)$$
$$V = (X - 100)\ln\left(1 - \frac{X}{100}\right)$$

where *k* is the relative hydraulic conductivity at *X*% loss of conductivity, k_{sat} is the saturated hydraulic conductivity (i.e. *k* at 0 MPa), *P* is the positive-valued xylem water potential ($P = -\Psi$), P_x is the Ψ at *X*% loss of conductivity, and S_x is the slope of the vulnerability curve at $P = P_x$. P_{50} was defined as Ψ at 50% loss of conductivity. Equation 3 was fit using nonlinear least squares (function nls in R 3.0.1; R Core Team, 2013). A bootstrap resampling technique was employed to calculate confidence intervals for the fitted parameters by fitting the curve to resampled data (999 replicates). The fitting routines were implemented as an R package (fitplc; available from Duursma, 2014). Curves were fitted separately for each sample run in centrifuge data with P_{50} and slope parameters, then calculated as the means of three to five replicates. In the Cavitron centrifuge data, *Q. robur* exhibited a double curve. Therefore, Weibull curves were fitted separately for each half of the curve in order to improve the estimation of P_{50} (Cai et al., 2014).

Vessel Lengths

The number of vessels open at both ends of a 0.275-m segment was measured by injection of silicone elastomer (Rhodorsil RTV 141; Rhodia), with a fluorescent optical brightener (Ciba Uvitex OB; Ciba Specialty Chemicals) mixed with chloroform (1%, w/w) and added to the silicone (Lens et al., 2011). Measurements were made on three stems of *Q. robur* and *P. tremula* × *P. alba*. Stems were sealed in a pressure manifold with one cut end submerged in elastomer. Samples were infiltrated at a pressure of 0.1 MPa for 24 h and then oven dried at 70°C overnight. Vessels were counted at both ends of the stem, with the difference between the proximal and distal ends representing the proportion of vessels cut open at both ends of the sample.

Supplemental Data

The following supplemental materials are available.

Supplemental Figure S1. Transverse slices from microCT scans show embolized and functional xylem conduits for well-hydrated samples of *Q. robur*, *P. tremula* × *P. alba*, and *P. pinaster*.

Supplemental Figure S2. Sequential images from microCT scans showing the effects of repeated scans and removal of leaves for water potential measurements.

Supplemental Figure S3. Vulnerability to drought-induced embolism in *Q. robur* saplings using two centrifuge techniques.

ACKNOWLEDGMENTS

We thank the Paul Scherrer Institute for the provision of synchrotron radiation beamtime at the TOMCAT beamline; Sarah Irvine and Kevin Mader for assistance with measurements at the TOMCAT beamline; the SOLEIL synchrotron for the provision of beamtime at the PSICHÉ beamline; Andrew King for assistance with measurements at the PSICHÉ beamline; Andrew McElrone for supplying a specialized plant holder for measurements at the SLS; Craig Brodersen for advice on image analysis and three-dimensional rendering; and Gaëlle Capdeville for assistance with static centrifuge measurements made in 2015.

Received May 18, 2015; accepted October 30, 2015; published November 2, 2015.

LITERATURE CITED

Alder NN, Pockman WT, Sperry JS, Nuismer S (1997) Use of centrifugal force in the study of xylem cavitation. J Exp Bot **48:** 665–674

Anderegg WRL (2015) Spatial and temporal variation in plant hydraulic traits and their relevance for climate change impacts on vegetation. New Phytol **205:** 1008–1014

Awad H, Barigah T, Badel E, Cochard H, Herbette S (2010) Poplar vulnerability to xylem cavitation acclimates to drier soil conditions. Physiol Plant **139:** 280–288

Brodersen CR, McElrone AJ, Choat B, Lee EF, Shackel KA, Matthews MA (2013) In vivo visualizations of drought-induced embolism spread in *Vitis vinifera*. Plant Physiol **161:** 1820–1829

Brodersen CR, McElrone AJ, Choat B, Matthews MA, Shackel KA (2010) The dynamics of embolism repair in xylem: in vivo visualizations using high-resolution computed tomography. Plant Physiol **154:** 1088–1095

Brodribb TJ, Cochard H (2009) Hydraulic failure defines the recovery and point of death in water-stressed conifers. Plant Physiol **149:** 575–584

Cai J, Li S, Zhang H, Zhang S, Tyree MT (2014) Recalcitrant vulnerability curves: methods of analysis and the concept of fibre bridges for enhanced cavitation resistance. Plant Cell Environ **37:** 35–44

Charra-Vaskou K, Badel E, Burlett R, Cochard H, Delzon S, Mayr S (2012) Hydraulic efficiency and safety of vascular and non-vascular components in Pinus pinaster leaves. Tree Physiol **32:** 1161–1170

Choat B (2013) Predicting thresholds of drought-induced mortality in woody plant species. Tree Physiol **33:** 669–671

Choat B, Brodersen CR, McElrone AJ (2015) Synchrotron x-ray microtomography of xylem embolism in *Sequoia sempervirens* saplings during cycles of drought and recovery. New Phytol **205:** 1095–1105

Choat B, Cobb AR, Jansen S (2008) Structure and function of bordered pits: new discoveries and impacts on whole-plant hydraulic function. New Phytol **177:** 608–625

Choat B, Drayton WM, Brodersen C, Matthews MA, Shackel KA, Wada H, McElrone AJ (2010) Measurement of vulnerability to water stress-induced cavitation in grapevine: a comparison of four techniques applied to a long-vesseled species. Plant Cell Environ **33:** 1502–1512

Choat B, Jansen S, Brodribb TJ, Cochard H, Delzon S, Bhaskar R, Bucci SJ, Feild TS, Gleason SM, Hacke UG, et al (2012) Global convergence in the vulnerability of forests to drought. Nature **491:** 752–755

Choat B, Lahr EC, Melcher PJ, Zwieniecki MA, Holbrook NM (2005) The spatial pattern of air seeding thresholds in mature sugar maple trees. Plant Cell Environ **28:** 1082–1089

Choat B, Sack L, Holbrook NM (2007) Diversity of hydraulic traits in nine *Cordia* species growing in tropical forests with contrasting precipitation. New Phytol **175:** 686–698

Christman MA, Sperry JS, Smith DD (2012) Rare pits, large vessels and extreme vulnerability to cavitation in a ring-porous tree species. New Phytol **193:** 713–720

Cochard H (2002) A technique for measuring xylem hydraulic conductance under high negative pressures. Plant Cell Environ **25:** 815–819

Cochard H, Badel E, Herbette S, Delzon S, Choat B, Jansen S (2013) Methods for measuring plant vulnerability to cavitation: a critical review. J Exp Bot **64:** 4779–4791

Cochard H, Cruiziat P, Tyree MT (1992) Use of positive pressures to establish vulnerability curves: further support for the air-seeding hypothesis and implications for pressure-volume analysis. Plant Physiol **100:** 205–209

Cochard H, Damour G, Bodet C, Tharwat I, Poirier M, Ameglio T (2005) Evaluation of a new centrifuge technique for rapid generation of xylem vulnerability curves. Physiol Plant **124:** 410–418

Cochard H, Delzon S, Badel E (2015) X-ray microtomography (micro-CT): a reference technology for high-resolution quantification of xylem embolism in trees. Plant Cell Environ **38:** 201–206

Cochard H, Herbette S, Barigah T, Badel E, Ennajeh M, Vilagrosa A (2010) Does sample length influence the shape of xylem embolism vulnerability curves? A test with the Cavitron spinning technique. Plant Cell Environ **33:** 1543–1552

Dalla-Salda G, Fernández ME, Sergent AS, Rozenberg P, Badel E, Martinez-Meier A (2014) Dynamics of cavitation in a Douglas-fir tree-ring: transition-wood, the lord of the ring? Journal of Plant Hydraulics **1:** e0005

Davis SD, Ewers FW, Sperry JS, Portwood KA, Crocker MC, Adams GC (2002) Shoot dieback during prolonged drought in Ceanothus (Rhamnaceae) chaparral of California: a possible case of hydraulic failure. Am J Bot **89:** 820–828

Dixon HH, Joly J (1895) On the ascent of sap. Philos Trans R Soc Lond B Biol Sci **186:** 563–576

Domec JC, Lachenbruch B, Meinzer FC (2006) Bordered pit structure and function determine spatial patterns of air-seeding thresholds in xylem of Douglas-fir (*Pseudotsuga menziesii*; Pinaceae) trees. Am J Bot **93:** 1588–1600

Duursma R (2014) Fit vulnerability curves in R (R package). https://bitbucket.org/remkoduursma/fitplc/

Ennajeh M, Simões F, Khemira H, Cochard H (2011) How reliable is the double-ended pressure sleeve technique for assessing xylem vulnerability to cavitation in woody angiosperms? Physiol Plant **142:** 205–210

Hacke UG, Venturas MD, MacKinnon ED, Jacobsen AL, Sperry JS, Pratt RB (2015) The standard centrifuge method accurately measures vulnerability curves of long-vesselled olive stems. New Phytol **205:** 116–127

Hoffmann WA, Marchin RM, Abit P, Lau OL (2011) Hydraulic failure and tree dieback are associated with high wood density in a temperate forest under extreme drought. Glob Change Biol **17:** 2731–2742

Holbrook NM, Ahrens ET, Burns MJ, Zwieniecki MA (2001) In vivo observation of cavitation and embolism repair using magnetic resonance imaging. Plant Physiol **126:** 27–31

Jacobsen AL, Pratt RB (2012) No evidence for an open vessel effect in centrifuge-based vulnerability curves of a long-vesselled liana (*Vitis vinifera*). New Phytol **194:** 982–990

Kaufmann I, Schulze-Till T, Schneider HU, Zimmermann U, Jakob P, Wegner LH (2009) Functional repair of embolized vessels in maize roots after temporal drought stress, as demonstrated by magnetic resonance imaging. New Phytol **184:** 245–256

Lens F, Sperry JS, Christman MA, Choat B, Rabaey D, Jansen S (2011) Testing hypotheses that link wood anatomy to cavitation resistance and hydraulic conductivity in the genus *Acer*. New Phytol **190:** 709–723

Li Y, Sperry JS, Taneda H, Bush SE, Hacke UG (2008) Evaluation of centrifugal methods for measuring xylem cavitation in conifers, diffuse- and ring-porous angiosperms. New Phytol **177:** 558–568

Martin-StPaul NK, Longepierre D, Huc R, Delzon S, Burlett R, Joffre R, Rambal S, Cochard H (2014) How reliable are methods to assess xylem vulnerability to cavitation? The issue of 'open vessel' artifact in oaks. Tree Physiol **34:** 894–905

McElrone AJ, Brodersen CR, Alsina MM, Drayton WM, Matthews MA, Shackel KA, Wada H, Zufferey V, Choat B (2012) Centrifuge technique consistently overestimates vulnerability to water stress-induced cavitation in grapevines as confirmed with high-resolution computed tomography. New Phytol **196:** 661–665

McElrone AJ, Choat B, Parkinson DY, MacDowell AA, Brodersen CR (2013) Using high resolution computed tomography to visualize the three dimensional structure and function of plant vasculature. J Vis Exp **74:** e50162

Melcher PJ, Meinzer FC, Yount DE, Goldstein G, Zimmermann U (1998) Comparative measurements of xylem pressure in transpiring

and non-transpiring leaves by means of the pressure chamber and the xylem pressure probe. J Exp Bot **49:** 1757–1760

Ogle K, Barber JJ, Willson C, Thompson B (2009) Hierarchical statistical modeling of xylem vulnerability to cavitation. New Phytol **182:** 541–554

Petty JA (1970) Permeability and structure of the wood of Sitka spruce. Proc R Soc Lond B Biol Sci **175:** 149–166

Pickard WF (1981) The ascent of sap in plants. Prog Biophys Mol Biol **37:** 181–229

Pittermann J, Choat B, Jansen S, Stuart SA, Lynn L, Dawson TE (2010) The relationships between xylem safety and hydraulic efficiency in the Cupressaceae: the evolution of pit membrane form and function. Plant Physiol **153:** 1919–1931

R Core Team (2013) R: A Language and Environment for Statistical Computing. R Foundation for Statistical Computing. http://www.R-project.org/ (June 1, 2014)

Rasband WS (2014) ImageJ. US National Institutes of Health, Bethesda, MD

Schenk HJ, Steppe K, Jansen S (2015) Nanobubbles: a new paradigm for air-seeding in xylem. Trends Plant Sci **20:** 199–205

Sperry JS, Christman MA, Torres-Ruiz JM, Taneda H, Smith DD (2012) Vulnerability curves by centrifugation: is there an open vessel artefact, and are 'r' shaped curves necessarily invalid? Plant Cell Environ **35:** 601–610

Sperry JS, Hacke UG, Pittermann J (2006) Size and function in conifer tracheids and angiosperm vessels. Am J Bot **93:** 1490–1500

Sperry JS, Tyree MT (1988) Mechanism of water stress-induced xylem embolism. Plant Physiol **88:** 581–587

Tobin MF, Pratt RB, Jacobsen AL, De Guzman ME (2013) Xylem vulnerability to cavitation can be accurately characterised in species with long vessels using a centrifuge method. Plant Biol (Stuttg) **15:** 496–504

Torres-Ruiz JM, Cochard H, Mayr S, Beikircher B, Diaz-Espejo A, Rodriguez-Dominguez CM, Badel E, Fernández JE (2014) Vulnerability to cavitation in *Olea europaea* current-year shoots: more support to the open-vessel artefact with centrifuge and air-injection techniques. Physiol Plant **152:** 465–474

Torres-Ruiz JM, Jansen S, Choat B, McElrone AJ, Cochard H, Brodribb TJ, Badel E, Burlett R, Bouche PS, Brodersen CR, et al (2015) Direct x-ray microtomography observation confirms the induction of embolism upon xylem cutting under tension. Plant Physiol **167:** 40–43

Torres-Ruiz JM, Sperry JS, Fernández JE (2012) Improving xylem hydraulic conductivity measurements by correcting the error caused by passive water uptake. Physiol Plant **146:** 129–135

Tyree MT (2003) Plant hydraulics: the ascent of water. Nature **423:** 923

Tyree MT, Davis SD, Cochard H (1994) Biophysical perspectives of xylem evolution: is there a tradeoff of hydraulic efficiency for vulnerability to dysfunction. IAWA J **15:** 335–360

Tyree MT, Sperry JS (1989) Vulnerability of xylem to cavitation and embolism. Annu Rev Plant Physiol Plant Mol Biol **40:** 19–38

Urli M, Porté AJ, Cochard H, Guengant Y, Burlett R, Delzon S (2013) Xylem embolism threshold for catastrophic hydraulic failure in angiosperm trees. Tree Physiol **33:** 672–683

Utsumi Y, Sano Y, Fujikawa S, Funada R, Ohtani J (1998) Visualization of cavitated vessels in winter and refilled vessels in spring in diffuse-porous trees by cryo-scanning electron microscopy. Plant Physiol **117:** 1463–1471

Wang MT, Tyree MT, Wasylishen RE (2013) Magnetic resonance imaging of water ascent in embolized xylem vessels of grapevine stem segments. Can J Plant Sci **93:** 879–893

Wang R, Zhang L, Zhang S, Cai J, Tyree MT (2014) Water relations of Robinia pseudoacacia L.: do vessels cavitate and refill diurnally or are R-shaped curves invalid in Robinia? Plant Cell Environ **37:** 2667–2678

Wei C, Tyree MT, Steudle E (1999) Direct measurement of xylem pressure in leaves of intact maize plants: a test of the cohesion-tension theory taking hydraulic architecture into consideration. Plant Physiol **121:** 1191–1206

Wheeler JK, Huggett BA, Tofte AN, Rockwell FE, Holbrook NM (2013) Cutting xylem under tension or supersaturated with gas can generate PLC and the appearance of rapid recovery from embolism. Plant Cell Environ **36:** 1938–1949

Zimmermann MH (1983) Xylem Structure and the Ascent of Sap. Springer-Verlag, New York

Zimmermann MH, Jeje AA (1981) Vessel-length distribution in stems of some American woody plants. Can J Bot **59:** 1882–1892